Surficial sediment remobilization by shear between sediment and water above tsunamigenic megathrust ruptures: experimental study

Chloé Seibert[1], Cecilia McHugh[2,1], Chris Paola[3], Leonardo Seeber[1], James Tucker[3]

[1]Lamont-Doherty Earth Observatory of Columbia University, Palisades New York, USA
[2]Queens College, City University of New York, School of earth and Environmental Sciences, New York 11367, USA
[3]Department of Earth and Environmental Sciences, St Anthony Falls Laboratory, University of Minnesota, Minneapolis, MN, USA

Correspondence to: Chloé Seibert (cseibert@umn.edu)

Abstract. Large subduction earthquakes can rupture the shallow part of the megathrust with unusually large displacements and tsunamis. The long duration of the seismic source and high upper-plate compliance contribute to large and protracted long-period motions of the outer upper plate. The resulting shear stress at the sediment/water interface in, for example, the Mw9.0 2011 Tohoku-Oki earthquake, could account for surficial sediment remobilization on the outer margin. We test this hypothesis by simulating in physical tank experiments the combined effects of high and low frequency seismic motions on sediment of different properties (chemistry, grain size, water content and salinity). Our results show that low-frequency motion during a 2011-like earthquake can entrain several centimeters of surficial sediment and that entrainment can be enhanced by high-frequency vertical oscillations. These experiments validate a new mechanism of co-seismic sediment entrainment in deep-water environments.

1 Introduction

All known earthquakes in the ≥M9.0 class originated from subduction megathrusts and have generated major tsunamis. The last 100 years saw five of these events. Despite their major risks given their long duration and low-frequency shaking, they are still poorly understood, as demonstrated by the last two earthquakes in this class, the Mw9.3 2004 Sumatra-Andaman and the Mw9.0 2011 Tohoku-Oki events (Lay, 2015). They ruptured the shallowest portion of the megathrust, which had been considered aseismic and was responsible for their catastrophic tsunamis. Constraining global hazard requires identifying subduction boundaries capable of producing very large earthquakes and determining their recurrence. Characterization of earthquake event deposits in the offshore sedimentary record is challenging (Talling, 2021) but has extended earthquake catalogs into pre-history and improved seismic hazard estimations along several active margins (e.g. Goldfinger et al., 2003, 2012; Pouderoux et al., 2014; Ratzov, et al., 2015; Usami et al., 2018; Seibert et al., 2024). Current work aims to relate distinctions among event deposits with earthquake characteristics such as magnitude and source locations (Goldfinger et al., 2013; Moernaut et al., 2017; Van Daele et al., 2019; McHugh et al., 2020; Howarth et al., 2021).

a supprimé: ldeo.columbia

a supprimé: megathrust

a supprimé: that

a supprimé: interface can cause

a supprimé: co-seismic

a supprimé: .

a supprimé: the

a supprimé: identified

a supprimé: Through

a supprimé: , we test this hypothesis by exploring shear between sediment and water, interactions between

a supprimé: waves, and

a supprimé: originate

a supprimé: boundaries.

a supprimé: high tsunamigenic risk, such earthquakes

a supprimé: Five events of this size have been experienced in the last century, but the lack of data about them leads to two critical needs for constraining

a supprimé: : 1)

a supprimé: ;

a supprimé: 2)

a supprimé: the

a supprimé: of these events

As one of the most instrumented in history, the Tohoku-Oki earthquake and tsunami provided detailed ground-truths related with specific sedimentary processes, including: a persistent deep sediment suspension (Noguchi et al., 2012; Oguri et al., 2013); tsunami-remobilized sediment possibly sourcing turbidity currents to the upper slope (Arai et al., 2013; Toyofuku et al., 2014; Tamura et al., 2015; Usami et al., 2017); large slumps at the trench (Kodaira et al., 2012; Strasser et al., 2013); turbidity flows originating on the slope and trench (Ikehara et al., 2014, 2016; Molenaar et al., 2019); and surficial sediment remobilization over ~100's of km^2 of the outer margin, including the mid-slope terrace and trench (McHugh et al., 2016, 2020). McHugh et al. (2016) document this process using short-lived radioisotopes. They highlight 2011-event deposits, some of which contain a basal turbidite overlain by a homogeneous muddy flow deposit (3-200cm-thick). These deposits are enriched in excess (xs)^{210}Pb that hasn't decayed and contain ^{137}Cs and ^{134}Cs derived from Fukushima. They argue that the thickness and spatial extend of these deposits required a sediment source widespread yet limited to the upper few cm of sediment. McHugh et al., (2020) hypothesize that this widespread surficial sediment entrainment is related to the large-amplitude, long-period seismic motion on the outer upper plate. Seafloor motion from large subduction earthquakes could be so large that it could move the bed relative to ambient water fast enough to create sufficient shear stress to entrain sediment, as suggested by Gomberg (2018). It is well established that seafloor shaking affects sediment, raising pore pressure and triggering mass movement and sediment density flows. However, shear stress induced by co-seismic seafloor motion is a new mechanism for sediment entrainment during earthquakes. In effect, it inverts conventional sediment dynamics, where the premise is that the bed is fixed, and the fluid moves relative to it. The implication for paleoseismology is that large megathrust earthquakes could mobilize sediment where that would otherwise be unlikely, creating distinctive sedimentary signatures.

The main purpose of this work is to test whether long-period seismic motion in subduction earthquakes that rupture to the trench can develop sufficient water-sediment differential velocity and shear stress to entrain the surficial sediment and investigate the consequences of its interaction with high-frequency vertical acceleration. From published results about the 2011 M9.0 rupture, we estimate the co-seismic long-period motions on the Japan slope-trench margin, and we report on initial laboratory experiments testing their potential for entraining sediments. We believe these are the first experiments on entrainment that combine high-frequency shaking of the sediment with shear between sediment and water that captures the effects of long period motions, including the static displacement and elastic oscillations. These first-order experimental runs also provide initial observations on how sediment properties (grain size, mineralogy, water content and salinity) affect surficial sediment remobilization.

2 Conceptual model

The Tohoku-Oki earthquake ruptured the seismogenic depth range of the Japan erosional subduction boundary (Von Huene et al., 1994), down dip into the mantle and up-dip to the trench (Fig. 1A). The co-seismic slip tended to increase up-dip, reaching ~60m at the trench (Lay et al., 2011a; Fujiwara et al., 2011). Based on world observations, Lay et al. (2012) subdivide the subduction interface in depth domains that radiate seismically with distinct spectral characteristics (Fig. 1A). In the shallowest

a supprimé: Understanding event deposits starts with sediment entrainment. The premise in sediment dynamics has been that the bed is fixed, and the fluid moves relative to it, creating shear stress that entrains sediment. Seafloor motion from large subduction earthquakes can be so large that alone could move the bed relative to ambient water fast enough to entrain sediment (Gomberg, 2018). The implication for paleoseismology is that large megathrust earthquakes could mobilize sediment in places where that would otherwise be unlikely, creating distinctive sedimentary signatures. ¶

a supprimé: to relate

a supprimé: signatures

a supprimé: a

a supprimé: documented

a supprimé: mechanism

a supprimé: highlighted

a supprimé:

a supprimé: consisting

a supprimé: from

a supprimé: to 200 cm

a supprimé: mud layers

a supprimé: has not

a supprimé: is in steady state, requiring

a supprimé: from

a supprimé: This source must also be widespread, to account for the thickness of the deposits. In addition to the Japan Subducti ... [1]

a déplacé (et inséré) [1]

a déplacé vers le haut [1]: McHugh et al.,

a supprimé: In

a supprimé: paper, we focus on

a supprimé: described in Japan (

a supprimé: 2016, 2020) and on

a supprimé: as a possible cause. The spectrum of seismic v ... [2]

a supprimé: , particularly

a supprimé: ones that include the slow-rupturing shallowes ... [3]

a supprimé: (e.g. Lay, 2015). This suggests that retrieving ... [4]

a supprimé: sediment records may open opportunities to ... [5]

a supprimé: . We

a supprimé: entire brittle

a supprimé: . From its nucleation, this rupture propagated both

a supprimé: displacement increased

a supprimé: 60 m

a supprimé: in Japan and elsewhere

a supprimé: subdivided

of these megathrust domains, the rupture radiates preferentially at low frequencies (Lay et al., 2011b). This rupture domain underlies the outer part of the upper plate, where low rigidity (Fig. 1) and low seismic velocities (Kodaira et al., 2017) independently characterize it as compliant. Seismic attenuation in the outer upper plate is likely to be high due to the presence of fluids rising from the subduction channel (e.g. Escobar et al., 2019), but it is generally proportional to frequency and is ineffective at long periods. Figure 1 points to the two components of the 2011 mainshock motions on the outer upper plate: A) the huge (~60m) oceanward 'static' displacement of the outer upper plate mostly accomplished at the onset of these motions; and B) resonance effects, which may locally amplify both amplitude and duration at specific periods.

Along ~100km of the outer ~50km of the Japan margin, the 2011 static horizontal displacements at the seafloor (Fujiwara et al., 2011) and slip at the megathrust (Yue & Lay, 2011, 2013) are both about ~50m, primarily horizontal and to the east (Fig. 1). The largest unidirectional motion at the seafloor can be as much as 65m because it includes also a dynamic overshoot up to 30% of the static displacement (e.g. Yue & Lay, 2011, Fig. 1A). This seafloor motion is primarily driven by the slip on the patch of the megathrust below it, which is accomplished in about ~40s at any one point on that rupture. The rupture propagates across the area in ~20s (Yue & Lay, 2011; Fig. 1B). Given the gentle average slope of the outer margin (Fig. 1B) and assuming that the water column above it moves only upward (e.g. Fujiwara et al., 2011), the relative motion between water and the uppermost sediment is expected to be nearly equal to the motion of the seafloor and to produce shear velocities ~1m/s during the ~1 minute of the first motion.

The dynamic overshoot initiates a seismic reverberation that follows the first motion. Enhancements of amplitude and duration of reverberation in narrow frequency bands are typical of sedimentary basins where seismic velocities are lower than the surroundings, but they have recently been also recognized at active margins by in-situ deep-water measurements of long-period teleseismic waves (Nakamura et al., 2015; Gomberg, 2018), where seismic velocities are similarly low due to accretion of water-rich sediment and tectonic deformation (e.g. Kodaira et al., 2020). Polarization, period and amplitude of this reverberation depend on the motion that initiates it, and on the geometry and seismic velocity structure of the upper plate, which informed the crude first-order model in Figure 1B. Based on available seismic velocities (Vp model Kodaira et al., 2017), we calculate the fundamental resonance periods of horizontally polarized shear waves (Fig. 1B and Supplementary 1). Upper plate thickens and average seismic velocities increase landward. Their compensating effects maintain the period close to ~10s over a ~20km wide belt of the outer margin centered on the mid-slope terrace (Fig. 1B), which possibly allows this large portion of the upper plate to oscillate coherently. The duration of the reverberation depends primarily on how little of the energy is absorbed by inelastic components of the deformation. The large and long-lasting elastic deformation that drove the huge 2011 displacement may signal a complex rheology that allows low attenuation at long periods in the outer upper plate despite low seismic velocities and rigidity. In conclusion, the reverberation of the outer upper plate excited by the 2011 mainshock rupture is likely to contribute significantly to the entrainment of sediment by the first motion.

a supprimé: margin
a supprimé: the upper plate.
a supprimé: is proportional to frequency and
a supprimé: it
a supprimé: contributing further
a supprimé: a spectral shift toward the
a supprimé: period at the sea floor. An important contribution
a supprimé: long-period oscillations
a supprimé: seafloor, however, may come from the resonance coupling between a horizontally polarized fundamental shear mode of oscillation of
a supprimé: -
a supprimé: wedge and
a supprimé: this wedge during rupture (Fig. 1A).
a supprimé: In an area ~50 km wide from
a supprimé: trench on
a supprimé: upper plate (Fig. 1B) and ~100 km along it
a supprimé: 50 m. Low rigidity and possible inelastic relaxation of the upper plate (G. Ekstrom personal communication) may account for the lack of attenuation and large size of the displacement. In addition, the first
a supprimé: includes a dynamic component that
a supprimé: Thus, the initial eastward displacement of the seafloor at the outer margin could have been ~65 m.
a supprimé: displacement
a supprimé: . This displacement
a supprimé: 40 seconds and the
a supprimé:
a supprimé: our Figure 1B in ~20 seconds
a supprimé:). Thus ~1 m/s is a reasonable estimate of the
a supprimé: velocity of the seafloor above the outer wedge during its ~60 seconds first pulse of eastward displacement. This pulse includes the static displacement and a dynamic overshoot, whi ... [6]
a supprimé: should
a supprimé: on the upper plate, producing
a supprimé: 1 m
a supprimé: This
a supprimé: may be extended if peak velocities in the early ... [7]
a supprimé:). Lower
a supprimé: at outer active margins are usually ascribed
a supprimé: The main purpose
a supprimé: work is to test whether such long-period motio ... [8]
a supprimé: (Gomberg, 2018).

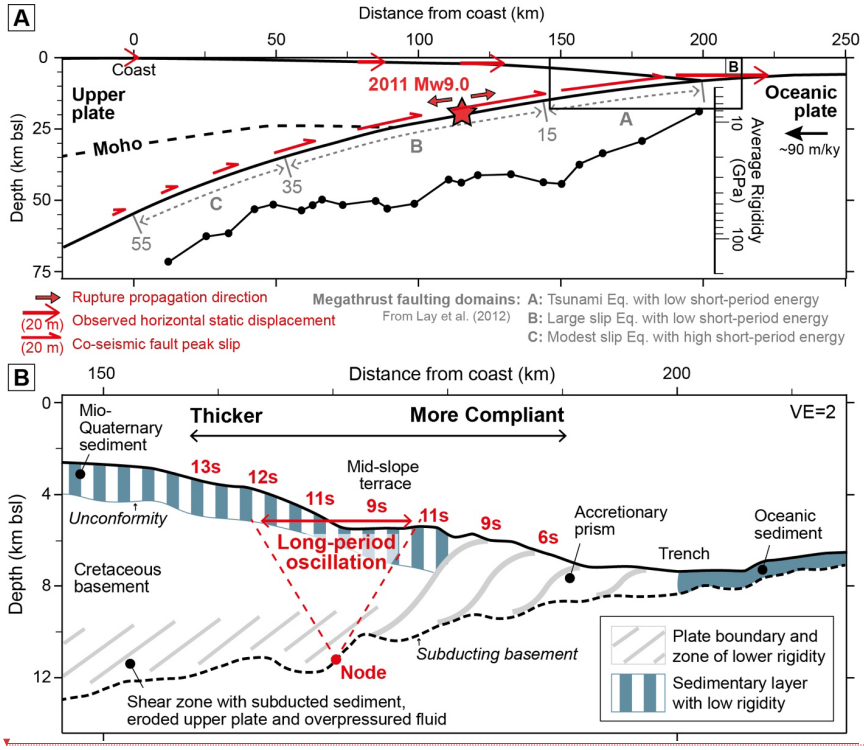

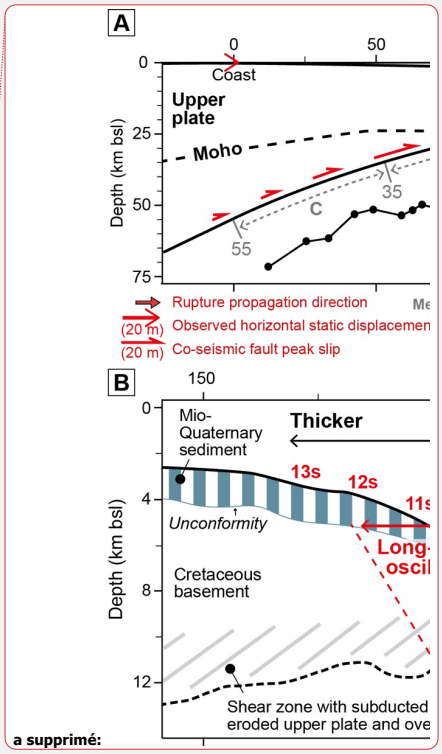

a supprimé:

235 **Figure 1: Profile across the Japan active margin at the 2011 Mw9.0 Tohoku-Oki megathrust rupture. A. Schematic cross section showing hypocenter and rupture initiation (red start) and megathrust domains A, B and C modified from Lay et al. (2012). Mean values of rigidity in depth bins from seismic-rupture radiation averaged for a number of megathrusts (Lay and Bilek, 2007). Note order of magnitude increase across the seismogenic range. Red half-arrows show peak co-seismic slip from Lay et al. (2012). Red arrows show the horizontal static displacement from Yue and Lay (2013). B. The outer upper plate above the largest 2011 rupture** 240 **displacements (based on MCS profile D11 from Kodaira et al., 2017). In red, periods of fundamental-mode horizontally polarized oscillation with nodes at the top of the subducting slab and "crests" at the seafloor (Supplementary 1). The landward increases in wedge thickness and S-wave velocity (i.e., rigidity; Von Huene et al., 1994; Fujiwara et al., 2011) allow for a ~20km wide plateau in fundamental periods at ~10s centered on the Mid-Slope Terrace.**

a supprimé:) (no vertical exaggeration

a mis en forme : Couleur de police : Bleu

a supprimé:). Periods

a supprimé: (red) (Fig. S1

a supprimé: 10 sec

3 Physical experiment setup

Our experiments (Supplementary 2) simplify the full spectrum of earthquake motion into two essential components: 1) the shear at the sediment-water interface associated with ~1min long build-up of the permanent displacement and ensuing slow oscillations, simulated experimentally by steady flow of water over the sediment; and 2) high-frequency P-waves (1-10Hz), which are simulated by vertical shaking of water and sediment within a rectangular duct (Fig. 2).

We worked on two sediment mixtures made of fine sand, silt and clay; a sand-poor mixture consisting of 10% fine sand, 45% silt, and 45% clay, and a sand-rich mixture consisting of 40% fine sand, 30% silt, and 30% clay. The percentage of each grain size are relative to the total of the dry sediment. We also investigated the role of water, varying the freshwater content between 50 and 80% relative to the total weight of the mixture. To assess the impact of salinity in a series of experiments, we used sea water (containing 3.5% salt) in place of freshwater within the sand-rich mixture.

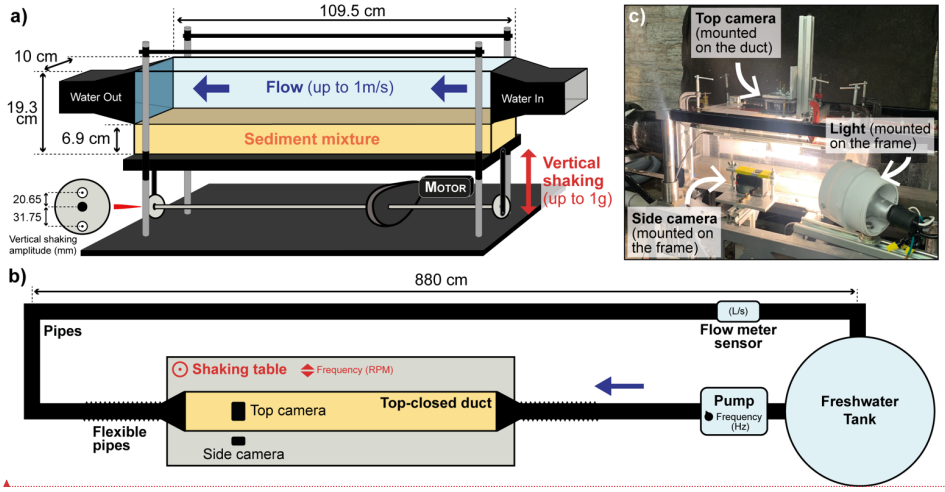

Figure 2: Physical experiment set up. a) Details of the duct with sediment and water. The shaking table amplitudes are set 20.65 mm or 31.75 mm for each run. b) Top view of the system. c) Photo of the downstream duct area targeted for data recording.

a supprimé: **Earthquake Motion**.
a supprimé: Text S1
a supprimé: quasi-steady
a supprimé: produced by the static
a supprimé: of the outer upper plate, which is
a supprimé: 10 Hz
a supprimé: 2a and 2b
a supprimé: **Sediment and water Composition**. Mixtures
a supprimé: -size bentonite simulated sediments. The first series of experiments used two sediment mixtures characterized by
a supprimé: low (10%) and high (40%)
a supprimé: content, with the remainder composed equally of
a supprimé: labelled Mix#1 and Mix#2, respectively (Table S1). We
a supprimé: with
a supprimé: ranging from
a supprimé: to
a supprimé: by
a supprimé: (implying 50 to 20% of sediment content
a supprimé: the mixture, respectively). We also did runs with Mix#
a supprimé: , which had the same dry sediment as Mix#2, but with saline rather than fresh water (Table S1).
a mis en forme : Anglais (E.U.)

4 Physical experiment results

The first set of experiments compared erosion rates caused by flow at different settings. The vertical peak acceleration, a_v, was either zero or constant at 1g during an entire run. The flow velocity, U, was set by switching the pump on at the start of the run and then remained steady. The mean velocity varied among the runs, ranging from 0 to 1m/s. We calculated erosion rates r in two ways: 1) by differencing bed topography before and after the run; and 2) by measuring from videos from one side of the duct. Both methods provide consistent results (Supplementary 3). We identified two processes of bed erosion: grain-by-grain, and stripping characterized by sudden entrainment of a cm-thick layer of sediment, as usual in such experiments.

For the sand-poor mix sediment with U=1m/s, erosion rates are low, ~0.03cm/min with grain-by-grain entrainment, regardless of water content and a_v (Fig. 3). Vertical shaking has no clear effect on entrainment rate even at a_v=1g. However, results for the sand-rich mixture depend on water content. With 50% and 60% freshwater and U=1m/s, r ranges from 0.008 to 0.029cm/min with predominantly grain-by-grain entrainment. With 70% freshwater and U=0.8m/s, we observe two phases (Supplementary 4): the first minutes show grain-by-grain entrainment and r_v=0.08-0.18cm/min; then the upper part of the bed is stripped, greatly increasing r, 1.3 and 1.5cm/min (Fig. 3 and Supplementary 3). With a flow velocity of 1m/s, the entire bed is eroded by stripping in 90s. With 80% freshwater and U=0.5m/s, r increases to 0.7-0.9cm/min (Fig. 3). There is no major stripping but sediment waves developed at the bed interface. With sea water in the sand-rich mixture, r increases dramatically, to 3cm/min with U=0.5 m/s (Fig. 3). Finally, for the same mixture (runs with 70 and 80% water) and flow velocity, erosion rates are higher when the sediment is subjected to a_v=1g (Fig. 3, Supplementary 3).

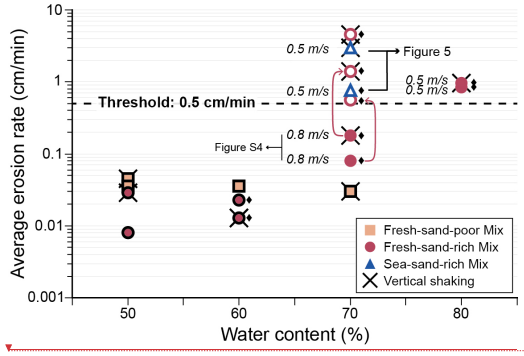

Figure 3: Entrainment versus sediment water content. Entrainment involves single grains only (full symbol), includes clumps of sediment (black diamonds), as above but with major rapid stripping (empty symbol). Each dot highlights the mean erosion rate over a run, but arrows link distinct erosion steps in the same run (the symbols at the start of the arrow show the mean erosion rate of the first step and the symbols at the end of the arrow show the mean erosion rate considering both steps). The crosses mark runs with a fixed vertical shaking at 3.5 Hz (with an amplitude of 20.65 mm) and an acceleration of 1 g. No shaking applied in other runs. The flow velocity was set up at a constant 1 m/s, unless specified. While the black outline indicates that the run lasted 10 min, the other runs were shorter due to the high erosion rates.

a supprimé: in…t different settings. Mean flow velocity U and The vertical peak acceleration, a_v were … was either zero or constant constant in each…t 1g during an entire run, but… The flow velocity, U, was set by switching the pump on at the start of the run and then remained steady. The mean velocity varied among the runs:… ranging from 0-1 m…to 1m/s and 0 or 1g respectively (Fig. 3).… We calculated erosion rates r_v… in two ways: 1) by differencing bed topography before and after the run; and 2) by measuring from videos from one side of the duct. Both methods provide consistent results (Table S2…upplementary 3). We identified two processes of bed erosion: 1) …rain-by-grain erosion;… and 2) stripping,…characterized by a …udden entrainment of a cm-thick layer of sediment. Once entrained by either mechanism, the sediment is transported out of the duct… as bedload and/or suspension ... [9]

a supprimé: Mix#1 and…ith U = …1m/s flow velocity… erosion rates are low, ~0.03 cm…3cm/min,…with grain-by-grain entrainment, regardless of water content and a_v (Fig. 3). Vertical shaking has no clear effect on entrainment rate even at a_v = …1g. Results…owever, results for Mix#2…he sand-rich mixture depend on water content. With 50% and 60% water content…reshwater and U = 1 m…1m/s, r_v… ranges from 0.008 to 0.029 cm…29cm/min with predominantly grain-by-grain entrainment. With 70 … freshwater and U = …0.8m/s, we observe two phases (Fig. S2…upplementary 4): the first minutes show grain-by-grain entrainment and r_v = …0.08 - …0.18 cm…8cm/min, Table S2);… then the upper part of the bed is stripped, greatly increasing r_v (…, 1.3 and 1.5 cm…cm/min, …(Fig. 3 and Table S2…upplementary 3). With a flow velocity of 1 m…m/s, the entire bed is eroded by stripping in 90 s…0s. With 80% water content, r_v for Mix#2…reshwater and U=0.5m/s, r increases to 0.7 - -0.9 cm…cm/min with U = 0.5 m/s …Fig. 3). There is no major stripping but sediment waves developed at the bed interface. With sea water in the sand-rich mixture (Mix#3), r_v,… r increases dramatically, to 3 cm…cm/min, even…with U = …0.5 m/s (Fig. 3). Finally, for the same mixture (runs with 70 and 80% water) and flow velocity, erosion rates are higher when the sediment is subjected to a_v = …1g (runs with 70 % and 80 % water on …ig. 3, Table S2 ... [10]

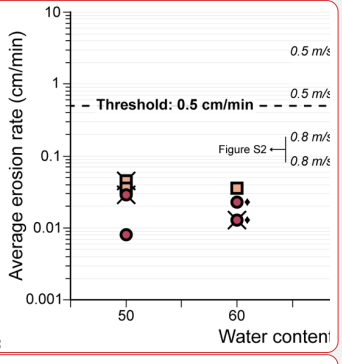

a supprimé:

a supprimé: ,

The results displayed on Figure 4 are the erosion rate for each sediment mixture with 70% water content. These runs were carried out without vertical shaking, and with gradually increasing flow velocity. Values of r for freshwater sediment mixture remain low (<0.1cm/min) but show distinct trends according to the sand content (Fig. 4A). For the sand-poor mixture, erosion starts with U=0.35m/s and increases up to 0.02cm/min at about 0.6m/s, but then remains constant. For the sand-rich mixture, erosion starts with a U=0.3m/s and increases up to 0.08cm/min at 0.8m/s. Figure 4B highlights the major impact of salinity on entrainment. Erosion rates at U=0.5m/s are 100 times higher for the sediment mixture with sea water than the mixtures with freshwater.

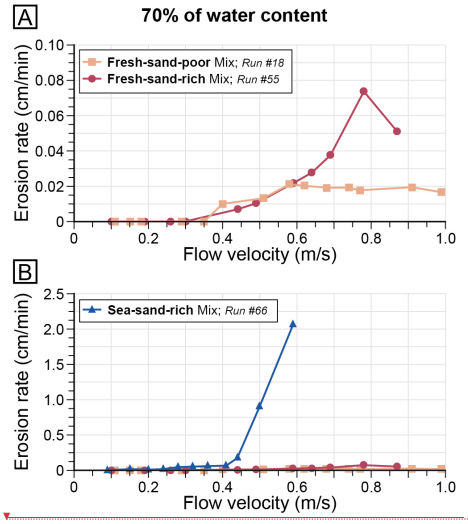

Figure 4: Evolution of the erosion rate for a representative run for the 3 mixtures, with a water content of 70 %, no vertical shaking and increasing the flow gradually. Plots A and B display the results for the same run with the fresh sand-poor and sand-rich mixtures, while an expanded vertical scale is used on plot B to highlight the results of the run with the sea-sand-rich mixture.

A closer look at the evolution of erosion rates over time for the sand-rich mixture with sea water shows the same trend with or without vertical shaking. During the first seconds, the sediment is eroded by stripping, leading to r values up to 13cm/min and 10.5cm/min for a_v=0 and 1g, respectively (Fig. 5). In a second phase, the erosion occurs grain-by-grain and via sediment clumps, with strong influence by the vertical shaking. With a_v=0, r ranges between 0.2 and 0.9cm/min (Fig. 5) and between 1.8 and 2.9cm/min for a_v=1g (Fig. 5).

a supprimé: compared …esults displayed on Figure 4 are the erosion rate versus flow velocity …or each of the three mixtures…ediment mixture with 70% water content is shown on Figure 4. The… These runs have no…ere carried out without vertical shaking, and a gradual increase of the…ith gradually increasing flow velocity. Values of r_v… for Mix#1 and Mix#2…reshwater sediment mixture remain low (< ….1cm/min) but show distinct trends according to the sand content (Fig. 4A). With Mix#1…or the sand-poor mixture, erosion starts with U = …0.35m/s and increases up to 0.02cm/min at about 0.6m/s, but then remains constant for velocities from 0.6 to 1.0 m/s. With Mix#2… For the sand-rich mixture, erosion starts with a U = …0.3m/s and increases up to 0.08cm/min at … [11]

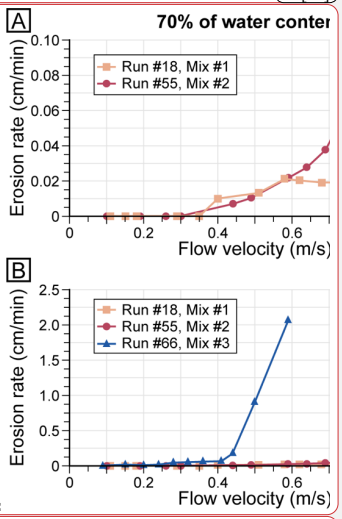

a supprimé:

a supprimé: 3… representative runs (one…un for each mixture…he 3 mixtures, with a water content of 70 %) with…, no vertical shaking and increasing the flow gradually. The plots…lots A and B show …isplay the results for the same curves for…un with the Mix#1…resh sand-poor and #2, but with…and-rich mixtures, while an expanded vertical scale for the M… [12]

a supprimé: Mix#3 runs…and-rich mixture with sea water shows the same trend with or without vertical shaking. During the first seconds, the sediment is eroded by stripping, leading to a_v… values up to 13 cm…3cm/min and 10.5 cm…cm/min for runs 67…$_v$=0 and 69…g, respectively (Fig. 5). In a second phase, the erosion occurs grain-by-grain and via sediment clumps, with strong influence by the vertical shaking. With a_v = …0, r_v… ranges between 0.2 and 0.9 cm…cm/min (Run 67, …ig. 5) and between 1.8 and 2.9 cm…cm/min for a_v = …1g (Run 69, … [13]

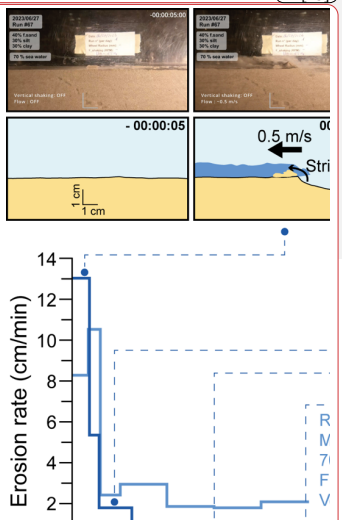

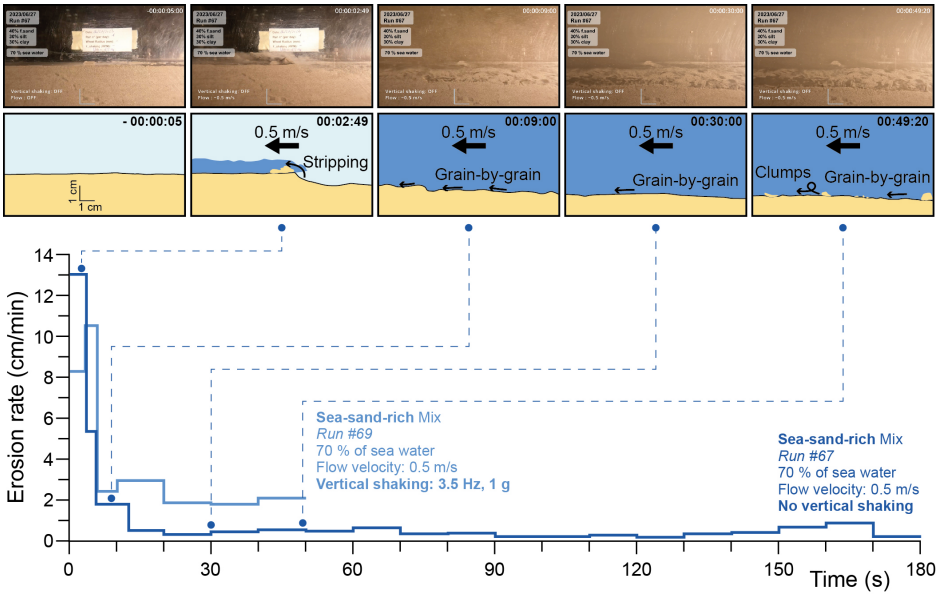

Figure 5: Evolution of the erosion rate of sea-sand-rich mixture. The erosion rates are calculated over 10 s-intervals but more often for the first ~10 seconds of each run. The photos and their interpretative cartoons highlight different steps of run #67.

a supprimé: Mix#3 sediment

5 Discussion and Conclusion

The initial results from our laboratory experiments show that the seafloor motion of the outer upper plate in response to the 2011 M9.0 rupture could cause widespread entrainment of surficial sediment with grain sizes and water contents consistent with the abyssal floor. Generally, our laboratory studies distinguish modes of remobilization that result from the interplay of high-frequency and low-frequency motions. They show that relative shear alone can effectively entrain surficial sediment and lead to the types of event deposits created by the 2011 earthquake. The short-lived radioisotopes measured from the submarine deposits demonstrated that the Tohoku-Oki earthquake triggered remobilization of the upper few centimeters of sediment over a wide area of the seafloor (McHugh et al., 2016). Based on this thickness and considering a duration ≥1 minute for the strong motion, including rupture and reverberation (Nakamura et al., 2015; Gomberg, 2018), we propose a threshold $\dot{\gamma}$ value of ~0.5cm/min, above which the erosion rate of surficial sediment is consistent with the field data (Fig. 3).

Our investigation of the surficial sediment entrainment under controlled conditions highlights that the intensity of the seismic waves is not the only factor determining whether sediment may be mobilized. The composition and the physical properties

a supprimé: experimental

a supprimé: we report here

a supprimé: between the seabed and water column compatible with a large rupture…

a supprimé: Tohoku-Oki

a supprimé: of several minutes

a supprimé: a_v

a supprimé: 5 cm

a supprimé: .

a mis en forme : Anglais (E.U.)

(e.g. water content, shear strength) of the sediment also strongly influence its susceptibility to entrainment. The results obtained with the sand-rich mixture show the impact of the water content on entrainment. Rapid entrainment by stripping occurs with ≥70% water, whereas erosion is insignificant below 70% (Fig. 3). In the field, the water content of the sediment decreases with increasing sediment burial due to compaction, typically reaching about 50% at a depth of 10-20cm. Thus, entrainment of surficial sediment by long-period motion is likely to be limited by the depth to more compacted sediment. Clay concentration and the ionic strength of the interstitial water (freshwater or sea water) are also significant factors (Fig. 4). Other parameters that could affect sediment entrainment include components like clay mineralogy, diatoms, ashes, organic matter biofilms, and also the nature and intensity of bioturbation.

The long-period motions (i.e. the quasi-steady flow in our experiments) can effectively remobilize relatively weak seafloor sediment on their own. But, for relatively weak, water-rich sediments, entrainment is enhanced by strong high-frequency vertical motions (a_v=1g) (Figs. 3 and 5). Our experiments do not include high-frequency shear wave motions, which might also contribute to remobilizing sediment.

a supprimé: Mix#2, enriched in
a supprimé: size particles,
a supprimé: Entrainment
a supprimé: in Mix#2
a supprimé: it
a supprimé: - 20 cm
a supprimé: sea-floor
a supprimé: its
a supprimé: PGA =

Acknowledgements

This work was funded by National Science Foundation OCE-2044915. We would like to acknowledge the support of Erik Steen, Chris Milliren and Erik Noren in the development of the experiment, and John Leeman from Leeman Geophysical for the construction of the shaking table. J. Gomberg, M. Clare and V. Sahakian are thanked for their comments which helped to improve the clarity of the manuscript.

Data availability

The data used for this manuscript are the recording videos of each run. Reduced-resolution copies of the videos are available at the following archival identifier: https://hdl.handle.net/11299/263944.

a supprimé:

Competing interests

The authors declare that they have no conflict of interest.

References

Arai, K., Naruse, H., Miura, R., Kawamura, K., Hino, R., Ito, Y., ... & Kasaya, T. (2013). Tsunami-generated turbidity current of the 2011 Tohoku-Oki earthquake. *Geology*, *41*(11), 1195-1198.

Ashi, J., Sawada, R., Omura, A., & Ikehara, K. (2014). Accumulation of an earthquake-induced extremely turbid layer in a terminal basin of the Nankai accretionary prism. *Earth, Planets and Space*, *66*(1), 1-9.

Escobar, M. T., Takahata, N., Kagoshima, T., Shirai, K., Tanaka, K., Park, J.-O., et al. (2019). Assessment of Helium Isotopes Near the Japan Trench 5 Years after the 2011 Tohoku-Oki Earthquake. ACS Earth Space Chem. 3, 581–587. doi:10.1021/acsearthspacechem.8b00190.

Fujiwara, T., Kodaira, S., No, T., Kaiho, Y., Takahashi, N., & Kaneda, Y. (2011). The 2011 Tohoku-Oki earthquake: Displacement reaching the trench axis. *Science*, *334*(6060), 1240-1240.

Goldfinger, C., Nelson, C. H., Johnson, J. E., & Shipboard Scientific Party. (2003). Holocene earthquake records from the Cascadia subduction zone and northern San Andreas fault based on precise dating of offshore turbidites. *Annual Review of Earth and Planetary Sciences*, *31*(1), 555-577.

Goldfinger, C., Nelson, C.H., Morey, A., Johnson, J.E., Gutierrez-Pastor, J., Eriksson, A.T., arabanov, E., Patton, J., Gracia, E., Enkin, R., Dallimore, A., Dunhill, G., Vallier, T., (2012). Turbidite Event History: Methods and Implications for Holocene Paleoseismicity of the Cascadia Subduction Zone. USGS Professional Paper 1661-F. U.S. Geological Survey, Reston, VA, p. 184, 64

Goldfinger, C., Ikeda, Y., Yeats, R. S., & Ren, J. (2013). Superquakes and supercycles. *Seismological Research Letters*, *84*(1), 24-32.

Gomberg, J. (2018). Cascadia onshore-offshore site response, submarine sediment mobilization, and earthquake recurrence. *Journal of Geophysical Research: Solid Earth*, *123*(2), 1381-1404.

Howarth, J. D., Orpin, A. R., Kaneko, Y., Strachan, L. J., Nodder, S. D., Mountjoy, J. J., ... & Cağatay, M. N. (2021). Calibrating the marine turbidite palaeoseismometer using the 2016 Kaikōura earthquake. *Nature Geoscience*, *14*(3), 161-167.

Ikehara, K., Irino, T., Usami, K., Jenkins, R., Omura, A., & Ashi, J. (2014). Possible submarine tsunami deposits on the outer shelf of Sendai Bay, Japan resulting from the 2011 earthquake and tsunami off the Pacific coast of Tohoku. *Marine Geology*, *358*, 120-127.

Ikehara, K., Kanamatsu, T., Nagahashi, Y., Strasser, M., Fink, H., Usami, K., ... & Wefer, G. (2016). Documenting large earthquakes similar to the 2011 Tohoku-oki earthquake from sediments deposited in the Japan Trench over the past 1500 years. *Earth and Planetary Science Letters*, *445*, 48-56.

Kodaira, S., No, T., Nakamura, Y., Fujiwara, T., Kaiho, Y., Miura, S., ... & Taira, A. (2012). Coseismic fault rupture at the trench axis during the 2011 Tohoku-oki earthquake. *Nature Geoscience*, *5*(9), 646-650.

Kodaira, S., Nakamura, Y., Yamamoto, Y., Obana, K., Fujie, G., No, T., ... & Miura, S. (2017). Depth-varying structural characters in the rupture zone of the 2011 Tohoku-oki earthquake. *Geosphere*, *13*(5), 1408-1424.

Kodaira, S., Fujiwara, T., Fujie, G., Nakamura, Y., & Kanamatsu, T. (2020). Large coseismic slip to the trench during the 2011 Tohoku-Oki earthquake. *Annual Review of Earth and Planetary Sciences*, *48*, 321-343.

Lay, T., & Bilek, S. (2007). Anomalous earthquake ruptures at shallow depths on subduction zone megathrusts. In *The seismogenic zone of subduction thrust faults* (pp. 476-511). Columbia University Press.

Lay, T., Ammon, C. J., Kanamori, H., Xue, L., & Kim, M. J. (2011a). Possible large near-trench slip during the 2011 M w 9.0 off the Pacific coast of Tohoku Earthquake. *Earth, planets and space*, *63*, 687-692.

Lay, T., Ammon, C. J., Kanamori, H., Yamazaki, Y., Cheung, K. F., & Hutko, A. R. (2011b). The 25 October 2010 Mentawai tsunami earthquake (Mw 7.8) and the tsunami hazard presented by shallow megathrust ruptures. *Geophysical Research Letters*, *38*(6).

Lay, T., Kanamori, H., Ammon, C. J., Koper, K. D., Hutko, A. R., Ye, L., ... & Rushing, T. M. (2012). Depth-varying rupture properties of subduction zone megathrust faults. *Journal of Geophysical Research: Solid Earth*, *117*(B4).

Lay, T. (2015). The surge of great earthquakes from 2004 to 2014. *Earth and Planetary Science Letters*, *409*, 133-146.

McHugh, C. M., Kanamatsu, T., Seeber, L., Bopp, R., Cormier, M. H., & Usami, K. (2016). Remobilization of surficial slope sediment triggered by the AD 2011 Mw 9 Tohoku-Oki earthquake and tsunami along the Japan Trench. *Geology*, *44*(5), 391-394.

McHugh, C. M., Seeber, L., Rasbury, T., Strasser, M., Kioka, A., Kanamatsu, T., ... & Usami, K. (2020). Isotopic and sedimentary signature of megathrust ruptures along the Japan subduction margin. *Marine Geology*, *428*, 106283.

Moernaut, J., Van Daele, M., Strasser, M., Clare, M. A., Heirman, K., Viel, M., ... & De Batist, M. (2017). Lacustrine turbidites produced by surficial slope sediment remobilization: a mechanism for continuous and sensitive turbidite paleoseismic records. *Marine Geology*, *384*, 159-176.

Molenaar, A., Moernaut J., Wiemer G., Dubois N., and Strasser M. (2019). Earthquake impact on active margins: tracing surficial remobilization and seismic strengthening in a slope sedimentary sequence. *Geophysical Research Letters* 46, no. 11: 6015-6023

Molenaar A., Van Daele M., Vandorpe T., Degenhart G., De Batist M., Urrutia R., Pino M., Strasser M., and Moernaut J. (2021). What controls the remobilization and deformation of surficial sediment by seismic shaking? Linking lacustrine slope stratigraphy to great earthquakes in South–Central Chile. *Sedimentology* 68, no. 6: 2365-2396.

Nakamura, T., Takenaka, H., Okamoto, T., Ohori, M., & Tsuboi, S. (2015). Long-period ocean-bottom motions in the source areas of large subduction earthquakes. *Scientific reports*, *5*(1), 16648.

Noguchi, T., Tanikawa, W., Hirose, T., Lin, W., Kawagucci, S., Yoshida-Takashima, Y., ... & Okamura, K. (2012). Dynamic process of turbidity generation triggered by the 2011 Tohoku-Oki earthquake. *Geochemistry, Geophysics, Geosystems*, *13*(11).

Oguri, K., Kawamura, K., Sakaguchi, A., Toyofuku, T., Kasaya, T., Murayama, M., ... & Kitazato, H. (2013). Hadal disturbance in the Japan Trench induced by the 2011 Tohoku–Oki Earthquake. *Scientific Reports*, *3*(1), 1915.

Pouderoux, H., Proust, J. N., & Lamarche, G. (2014). Submarine paleoseismology of the northern Hikurangi subduction margin of New Zealand as deduced from Turbidite record since 16 ka. *Quaternary Science Reviews*, *84*, 116-131.

Ratzov, G., Cattaneo, A., Babonneau, N., Déverchère, J., Yelles, K., Bracene, R., Courboulex, F. (2015) Holocene turbidites record earthquake supercycles at a slow-rate plate boundary. *Geology*; 43 (4): 331–334. doi: https://doi.org/10.1130/G36170.1

Seibert, C., Feuillet, N., Ratzov, G., Beck, C., Morena, P., Johannes, L., ... & Woerther, P. (2024). Sedimentary Records in the Lesser Antilles Fore-Arc Basins Provide Evidence of Large Late Quaternary Megathrust Earthquakes. *Geochemistry, Geophysics, Geosystems*, *25*(2), e2023GC011152.

Strasser, M., Kölling, M., Ferreira, C. D. S., Fink, H. G., Fujiwara, T., Henkel, S., ... & JAMSTEC Cruise MR12-E01 scientists. (2013). A slump in the trench: Tracking the impact of the 2011 Tohoku-Oki earthquake. *Geology*, *41*(8), 935-938.

Talling, P. J. (2021). Fidelity of turbidites as earthquake records. Nature geoscience, 14(3), 113-116.

Tamura, T., Sawai, Y., Ikehara, K., Nakashima, R., Hara, J., & Kanai, Y. (2015). Shallow-marine deposits associated with the 2011 Tohoku-oki tsunami in Sendai Bay, Japan. *Journal of Quaternary Science*, *30*(4), 293-297.

Toyofuku, T., Duros, P., Fontanier, C., Mamo, B., Bichon, S., Buscail, R., ... & Kitazato, H. (2014). Unexpected biotic resilience on the Japanese seafloor caused by the 2011 Tōhoku-Oki tsunami. *Scientific Reports*, *4*(1), 7517.

Usami, K., Ikehara, K., Jenkins, R. G., & Ashi, J. (2017). Benthic foraminiferal evidence of deep-sea sediment transport by the 2011 Tohoku-oki earthquake and tsunami. *Marine Geology*, *384*, 214-224.

Usami, K., Ikehara, K., Kanamatsu, T., & McHugh, C. M. (2018). Supercycle in great earthquake recurrence along the Japan Trench over the last 4000 years. *Geoscience Letters*, *5*(1), 1-12.

Van Daele, M., Araya-Cornejo, C., Pille, T., Vanneste, K., Moernaut, J., Schmidt, S., ... & Cisternas, M. (2019). Distinguishing intraplate from megathrust earthquakes using lacustrine turbidites. *Geology*, *47*(2), 127-130.

Von Huene, R., Klaeschen, D., Cropp, B., & Miller, J. (1994). Tectonic structure across the accretionary and erosional parts of the Japan Trench margin. *Journal of Geophysical Research: Solid Earth*, *99*(B11), 22349-22361.

Yue, H., & Lay, T. (2011). Inversion of high-rate (1 sps) GPS data for rupture process of the 11 March 2011 Tohoku earthquake (Mw 9.1). *Geophysical Research Letters*, *38*(7).

Yue, H., & Lay, T. (2013). Source rupture models for the M w 9.0 2011 Tohoku earthquake from joint inversions of high-rate geodetic and seismic data. *Bulletin of the Seismological Society of America*, *103*(2B), 1242-1255